Nonlinearity and ionization in Xe: Experiment-based calibration of a numerical model

J. Tolliver[1], S. Zahedpour[2], J. K. Wahlstrand[2,3], H. M. Milchberg[2], and M. Kolesik[1,*]

[1] College of Optical Sciences, University of Arizona, Tucson, Arizona 85712, USA
[2] Institute for Research in Electronics & Applied Physics, University of Maryland, College Park, Maryland 20742, USA
[3] Physical Measurement Laboratory, National Institute of Standards and Technology, Gaithersburg, MD 20899, USA
[*] Corresponding author: kolesik@acms.arizona.edu

Compiled September 11, 2020

Recently proposed universality of the nonlinear response is put to the test and used to improve a previously designed model for Xenon. Utilizing accurate measurements resolving the nonlinear polarization and ionization in time and space, we calibrate the scaling parameters of the model, and demonstrate agreement with several experiments spanning the intensity range relevant for applications in nonlinear optics at near-infrared and mid-infrared wavelengths. Applications to other species including small molecules are discussed, suggesting a self-consistent way to calibrate light-matter interaction models.

http://dx.doi.org/10.1364/ao.XX.XXXXXX

Computer-aided modeling in the realm of extreme nonlinear optics requires numerically efficient descriptions of light-matter interactions that can connect the quantum physics governing atoms and molecules, and the macroscopic dynamics of high-power optical pulses. Metastable Electronic State Approach (MESA) [1] represents a possible solution in certain situations. While the approach requires a one-time characterization of the given atom or molecule which must be done on the quantum-level, subsequent response evaluation is inexpensive, thus making large-scale simulations feasible even in situations that involve optical fields propagating over long distances (e.g. in optical filamentation [2–6]). Naturally, the fidelity of the MESA-based description is determined by the approximations built into the original quantum model. This work aims to address the question of possible improvements, or calibration with the help of suitable experimental data. In particular, we use measurements to improve a previously constructed model [7] for the nonlinear polarization and ionization of Xe.

The significance of the result goes beyond a concrete species or a particular modeling approach. Here we put to the first experimental test the idea that the nonlinear optical response can be described with universal functional forms. The fact that we can verify such a prediction against accurate measurements gives us a hope that similar model improvement can be applied to other species, including small molecules.

Moreover, the approach presented in this work should inform the practice of numerical modeling in extreme nonlinear optics, especially in the regimes where both bound and free electrons contribute to the optical response. Because the ionization rates are not known with a great accuracy, the corresponding model parameters are often treated as fitting parameters adjusted to a particular experiment. One take-away from this work is that such adjustments should not be done to the ionization model alone, but also the nonlinear polarization should be scaled accordingly as discussed in what follows. Such and approach recognizes that different aspects of the nonlinear response are intimately connected.

The method we build on in this work was tested against exact solutions [8] and results of TDSE simulations [9, 10], and was further compared to space-and-time resolved measurements [11, 12] of the nonlinear response in Argon and Krypton gases [13]. In the adiabatic regime, MESA [1, 13] describes an atom with two functions, $P_{\rm NL}(F)$ and $\Gamma(F)$, that give, respectively, the nonlinear induced dipole moment and the ionization rate caused by electric field F. These functions are obtained from the Stark resonance $\psi_0(F)$ related to the electronic bound state at $F=0$. If $E_0(F)$ is its Stark-shifted complex-valued energy, then $\Gamma = 2{\rm Im}\{E_0\}$, and $P_{\rm NL}$ can be obtained from the real part as

$$P_{\rm NL} = P(F) - \lim_{s\to 0} P(sF)/s \quad , \quad P(F) = -\partial_F E_0(F)\,. \qquad \textbf{(1)}$$

Alternatively, $P(F)$ can be calculated as a generalized expectation value for the dipole moment [14]. In the adiabatic approximation suitable for longer wavelengths, the response only depends on the value of the field, but not on its history.

For wavelengths shorter than about two microns, post-adiabatic corrections [10] can be included to obtain wavelength-dependent ionization rates. The resulting post-adiabatic correction of the ionization rate is then proportional to the square of the frequency, and characterized by the field-strength dependent function $M(F)$ also obtained from the metastable state;

$$\delta\Gamma \sim F'(t)^2 \frac{M(F(t))}{E_{\rm eff}} \quad , \quad M(F) = {\rm Im}\langle \partial_F \psi_0(F) | \partial_F \psi_0(F)\rangle\,. \qquad \textbf{(2)}$$

Here $E_{\rm eff}$ arises when a memory function is approximated by a decaying exponential, and it is treated as an adjustable parameter [13].

Our goal for this paper is to take the previously calculated model for Xe [7] and calibrate it with the help of measurements. The experimental inputs used here are based on the Single-shot Supercontinuum Spectral Interferometry (SSSI). Various aspects of this technique were discussed elsewhere [12, 15–21], and the experiments that produced the data utilized in the present work were described in Ref. [13] together with their numerical modeling.

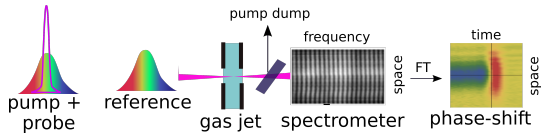

Fig. 1. Simplified schematic of the SSSI experiment.

The SSSI measurement uses three pulses (see Fig. 1 for a simplified schematic); pump, probe, and a reference, all interacting with a thin gas jet, the short interaction length minimizing the propagation effects. The reference pulse is identical to the probe, but is advanced so that it samples the jet alone and serves as a phase reference. The pump and the probe propagate through the gas jet together, and the intense pump "imprints" the phase change caused by the nonlinear interaction(s) on the probe. The chirp of the probe realizes time-to-frequency mapping, where a phase shift induced for a given wavelength corresponds to the nonlinear interaction in the time-slice of the pump that overlaps with that wavelength of the probe. As a result, the probe and the reference carry different phase profiles as they exit the gas jet. They are analyzed in an imaging spectrometer, producing a spectrogram for each transverse point of the beam imaged onto the spectrometer slit. The probe-reference phase difference is obtained from the spectrogram and this is the nonlinear phase shift mapped as a function of the position in the cross-section of the beam and the local time in the pulse. We refer the reader to Ref. [13] for details of the experiment. The simulation of the measurement includes the three pulses and models the whole experiment in detail, utilizing the unidirectional pulse propagation equation [22] solver [23].

Data from six separate experiments executed at different peak-power of the pump pulse are used here. Each measurement set provides a three-dimensional map of the nonlinear phase shift experienced by the optical pulse in a thin Xenon gas jet. The resolution achieved in these experiments is a few microns in two spatial dimensions spanning the transverse profile of the beam, and a few femtoseconds along the temporal axis of the pulse. Importantly, these experiments explore a range of optical intensities 20-80TW/cm^2 in which nonlinear focusing and strong-field ionization simultaneously affect the dynamics of the optical pulse and can not be considered in isolation. This is precisely the regime relevant for optical filamentation and extreme nonlinear optics in general.

We have previously used similar data obtained for Argon and Krypton to verify their corresponding MESA-based models [13]. While the agreement for these species was found to be good, we have also detected deviations between the experiment and the theory in the case of Xenon. We speculate that the results were less accurate because Xe is heavier and significantly more nonlinear. It is our aim here to revisit and improve the Xenon model, taking advantage of the recently discussed properties of the nonlinear response in noble gases.

Based on a numerical study we have have found that the nonlinear optical response of noble-gas atoms can be described in a unified form [7] given by

$$P_{\rm nl}^{(a)}(F) = \alpha_a^3 \mathcal{F}^3 M(\mathcal{F}), \quad \Gamma^{(a)}(F) = \alpha_a G(\mathcal{F}), \tag{3}$$

where two scaling parameters α_a and β_a are specific for each atom, the scaled field strength $\mathcal{F} = \beta_a F$, and universal functions $M(\mathcal{F})$ and $G(\mathcal{F})$ represent the nonlinear induced dipole and the ionization rate, respectively. Important for this work is that while different models of an atom (e.g. realized with different single active electron potentials [24, 25]) may give different values for the response, the functional shape turns out to be quite robust [7]. In other words, while a model may get the scale wrong, the functional shape of the response can still be close to the "master curves" $M(F)$, $G(F)$. This realization invites us to try to find appropriate scaling parameters $\alpha_{\rm Xe}$ and $\beta_{\rm Xe}$ from a comparison with an experiment, while keeping the the master curves unchanged.

We have chosen one of the experiments, labeled #10 at pump peak intensity between 44.6-50.4 TW/cm^2, as a "target" to adjust the scaling parameters of Xenon originally obtained from the theory. We want to emphasize that the choice of the concrete experiment to serve as the reference is not essential, as long as the peak intensity is in the range that will cause some plasma generation besides self-focusing. We have chosen this particular experiment based on the low level of noise. The reason that different experiments give us similar results when used as a reference is simply the fact that each SSSI measurement encompasses a range of intensities. In other words, a single SSSI experiment in fact represents a multitude of measurements achieved in a single shot.

Different SSSI experiments are distinguished by their peak pulse intensity. Here and below we quote a range of values for each, and the range represents two different measurement methods used. One is based on a calibration using the known value of nonlinear index for Argon (we refer to it as method 1), and the other used comparison with the orientational part of n_2 in molecular Oxygen [20] (method 2).

In order to express the adjustment as a modification of the original theoretical parameters, we replaced

$$\alpha_{\rm Xe} \to a\alpha_{\rm Xe} \quad \beta_{\rm Xe} \to b\beta_{\rm Xe} \tag{4}$$

in the formulas specified in Ref. [7]. A large number of simulations of the experiment were executed varying calibration values a, b in a vicinity of unity. For each simulation run, we evaluated a merit function $\sum_{i,j}[(\phi_{\rm exp}(\vec{r}_i, t_j) - (\phi_{\rm sim}(\vec{r}_i, t_j)]^2$ and selected the set of parameters that minimized this difference between the experimental and simulated nonlinear phase-shift. This is how we arrived at $a = 0.91$, $b = 0.99$, the values that represent the required adjustment of the theoretical $\alpha_{\rm Xe}$, $\beta_{\rm Xe}$. The uncertainty is about one percent, which means that the adjustment in β is not important. However the adjustment of α modifies both the ionization and polarization parts of the response. In the same parameter-scanning process we also determined the optimal value for the post-adiabatic correction parameter $E_{\rm eff} = 0.63$, which value is in line with the results previously obtained for Ar and Kr [13]. Interestingly, different values of $E_{\rm eff}$ did not affect the optima for a, b very much. So the adjustment parameters are more or less orthogonal to each other and this gives us confidence that a, b in particular can be safely used at longer wavelengths where the post-adiabatic correction (2) is unnecessary.

Figure 2 illustrates how the measured and simulated nonlinear shifts compare as functions of the transverse position in the beam, and as functions of time. Panel a) shows what is the typical shape of the nonlinear shift, where the leading edge of the pulse is dominated by the focusing Kerr nonlinearity manifested in the positive phase shift that increases with the local intensity. At later times when free electrons contribute, the phase shift becomes negative in proportion to the density of freed electrons. Two surfaces are depicted in the figure, and we take advantage of the measurement noise to illustrate that the surfaces are indeed close to each other across the whole space-time domain. For a more quantitative view, panel b) shows the temporal line-out at a spatial point on the axis, demonstrating a good agreement between the simulation and experiment for a peak intensity at which the Kerr-effect and plasma-defocusing are comparable in strength. We also include a curve that represents the simulation with $a, b = 1$ (i.e. uncorrected original model), in order to show that a relatively small adjustment of the scaling parameters does affect the model response. The change is significant enough to turn a qualitative model into an accurate modeling tool.

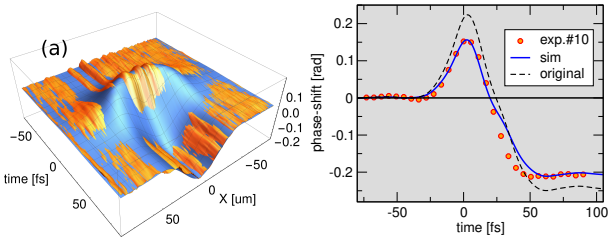

Fig. 2. Nonlinear phase shift in a pulse propagating across a Xenon gas jet. a) Blue (simulation) and orange (experiment) surface plots show a typical spatial-temporal phase-shift profile. b) The time-dependent phase shift for a spatial point on the beam axis. Data is for experiment #10, with the peak pump intensity measured in the range 46.5-50.4TW/cm^2. The full line represents the simulation result with the calibrated scaling parameters, while the dashed line shows the phase shift from the original model before calibration.

The remaining five experiments were used for out-of-sample tests. We kept the scaling parameters fixed at values obtained from fitting experiment #10, and executed simulations for the rest of SSSI runs. In what follows we demonstrate that the calibrated model can faithfully reproduce all the other measurements.

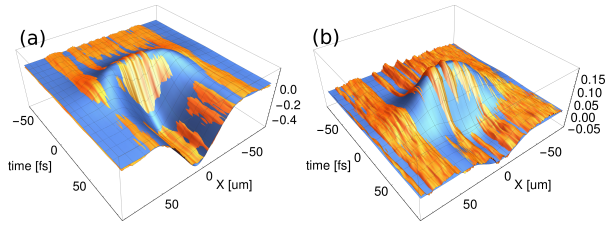

Fig. 3. Simulated (blue surface) and measured (orange surface) nonlinear phase shift for a pulse with peak intensity in the range of 57-62TW/cm^2 shown in (a) and 35-39TW/cm^2 in (b).

Figure 3 shows counterpart data to Fig. 2a) but for two experiments with higher and lower peak intensity of the pump pulse. In panel a) the phase-shift profile is dominated by the high intensity and therefore higher freed electron densities. The result is a depressed positive peak where Kerr and plasma compete, followed at later times by a deep ridge left in the wake of the pulse, which is due to the negative refractive index contribution caused by the plasma. Figure part b) is for a lower intensity where the plasma generation is weaker. Note that the leading edge peak is comparable to that shown in a) because it is less affected by the freed electrons. Overall in both cases the agreement is good.

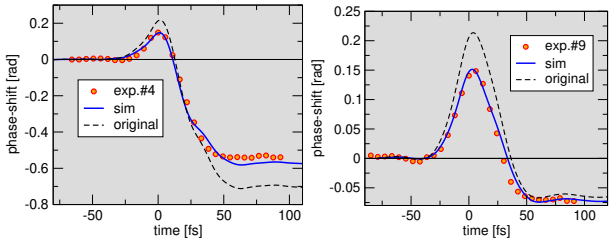

Fig. 4. Nonlinear phase shift as function of time taken at the on-axis spatial point. The peak measured intensity were 57-62TW/cm^2 and 35-39TW/cm^2 in (a) and (b), respectively.

Figure 4 shows the corresponding temporal line-outs for the spatial location on the beam axis. Here, again, the agreement is quite satisfactory. In the left panel a) we see a situation when the positive peak is a result of a partial cancellation between the Kerr effect and plasma-induced defocusing; in the absence of freed electrons, the peak would be significantly higher. The fact that the model can reproduce the correct value of the composite nonlinear shift is a witness to the capability of the MESA description to ensure the proper relative strength between the competing effects.

To complete our comparative illustrations, let us look at the two experiments with the lowest and highest peak pump intensity. Figure 5 depicts the transverse spatial profile of the measured and simulated phase shifts at a low (a) and high (b) peak intensity. These graphs are made for local times that coincide with the peak of the pump. The shift in the former is almost fully due to the self-focusing nonlinearity, while the latter exhibits a competition with plasma. There one can see the positive phase shifts on the periphery of the beam where only relatively few electrons are generated, while the center shows strongly negative shift due to the high plasma density.

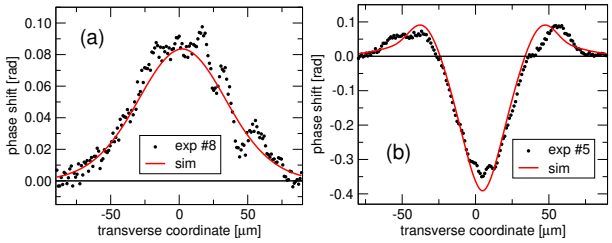

Fig. 5. Transverse profile of the nonlinear phase-shift for low peak intensity (a), 38-42TW/cm^2, and high intensity (b), 71-77TW/cm^2. These spatial line-outs are taken at the time corresponding to the temporal center of the pump pulse.

We trust the above data demonstrates that our calibrated model captures the nonlinear response of Xenon quite accurately and across different regimes. We finish with an additional observation, which concerns the measurement of the nonlinear peak intensity in experiments. It is often a subtle issue in

high-intensity experiments when the direct measurement is challenging due to both the ultrafast dynamics and very strong fields. The interesting point is that we do not need to know at exactly what nominal peak intensity of the pump was each experiment performed. This is because each of the experiments that we simulate encompasses parts of the pulse with strong as well as weak fields. Getting a good agreement for one peak pump power over the whole spatial-temporal extent of the pulse therefore means that the model should work accurately at all intensities.

To illustrate this observation, we have performed simulations of each experiment for a range of initial pump peak intensities, and we identified the value at which the best agreement was obtained for the given measurement. In other words, we pretend not to know the peak pump intensity and test if we can recover it from the measured data. The resulting "deduced" intensity is then compared with the values measured for the given experiment, and they turn out to agree nicely as is illustrated in Fig. 6. It shows two methods used to determine the intensity for each experiment compared to the peak intensity deduced from our simulations. Let us emphasize that while experiment #10 was used to calibrate the model, no further adjustments were allowed for other experiments. The fact that we can determine at what intensity was a given measurement done provides a further support for the model accuracy. It indicates that the calibration of the model could be achieved from a single SSSI experiment even if its peak intensity is not measured. It shows that the intensity, which is often difficult to know accurately, can be essentially by-passed, thus eliminating the potential error introduced by a biased peak intensity.

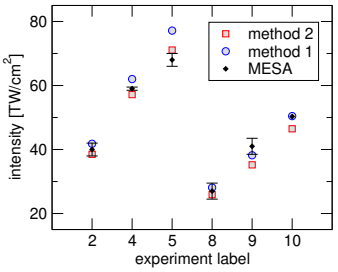

Fig. 6. Measured pump peak intensities compared to their values deduced from the simulations. The error bars in the simulated data roughly represent the interval over which an accurate fit to the measurement can be obtained. Square and circle symbols represent measurements utilizing different methods (see text).

In conclusion, we have tested against experiments the idea of a common functional form of the optical response in noble gases and used it to calibrate our previously calculated model for the nonlinear polarization and ionization of Xe exposed to a strong optical field. The method is based on the observation that while different quantum-mechanical models can provide quantitatively different answers for the nonlinear index and ionization rates, their functional dependence on the field strength is more robust. This allowed us to identify two scaling parameters which we adjusted so that a good match to a single SSSI experiment was achieved. Subsequently, we could demonstrate that such a calibrated model was able to accurately reproduce several other experiments over a wide range of peak pulse intensities. Thus, the values of the scaling parameters specific to Xenon determined in this work, together with the "master curves" for the nonlinear response published in Ref.[7] turn the original, merely qualitative model into a practical tool which is now accurately tested against state-of-the-art experiments.

Generally speaking, the approach, demonstrated here with Xenon, should be applicable to different species and with models of different designs. This is because the notion of the universal functional shape of the response depends on the asymptotic form of the potential experienced by an electron during the ionization process. This potential is, asymptotically, the superposition of a Coulomb and homogeneous electric fields, and it is common to all singly-ionized systems. In the vicinity of the "ionization path" of the electron, the potential appears approximately scale-invariant and this is the root of the similarity between different species. It is therefore conceivable that the scaling expressed in Eqn.(3) could be useful for other gases including air constituents. It should be interesting to test if similar model calibration with the help of experimental data could be done for molecular nitrogen or oxygen.

Funding. This material is based upon work supported by the Air Force Office of Scientific Research under award number FA9550-16-1-0121 and FA9550-18-1-0183.

Disclosures. The authors declare no conflicts of interest.

REFERENCES

1. M. Kolesik, J. M. Brown, A. Teleki, P. Jakobsen, J. V. Moloney, and E. M. Wright, Optica **1**, 323 (2014).
2. A. Couairon and A. Mysyrowicz, Phys. Rep. **441**, 47 (2007).
3. L. Bergé, S. Skupin, R. Nuter, J. Kasparian, and J.-P. Wolf, Rep. Prog. Phys. **70**, 1633 (2007).
4. J. Kasparian and J.-P. Wolf, Opt. Express **16**, 466 (2008).
5. S. L. Chin, Femtosecond Laser Filamentation (Springer, 2009).
6. S. L. Chin, T.-J. Wang, C. Marceau, J. Wu, J. S. Liu, O. Kosareva, N. Panov, Y. P. Chen, J.-F. Daigle, S. Yuan, A. Azarm, W. W. Liu, T. Seideman, H. P. Zeng, M. Richardson, R. Li, and Z. Z. Xu, Laser Phys. **22**, 1 (2012).
7. M. Kolesik and E. M. Wright, Opt. Express **27**, 25445 (2019).
8. J. M. Brown, A. Lotti, A. Teleki, and M. Kolesik, Phys. Rev. A **84**, 063424 (2011).
9. A. Bahl, J. M. Brown, E. M. Wright, and M. Kolesik, Opt. Lett. **40**, 4987 (2015).
10. A. Bahl, E. M. Wright, and M. Kolesik, Phys. Rev. A **94**, 023850 (2016).
11. J. K. Wahlstrand, Y.-H. Cheng, and H. M. Milchberg, Phys. Rev. Lett. **109**, 113904 (2012).
12. S. Zahedpour, J. K. Wahlstrand, and H. M. Milchberg, Opt. Lett. **40**, 5794 (2015).
13. A. Bahl, J. K. Wahlstrand, S. Zahedpour, H. M. Milchberg, and M. Kolesik, Phys. Rev. A **96**, 043867 (2017).
14. J. M. Brown and M. Kolesik, Adv. Math. Phys. **2015**, 125832 (2015).
15. K. Y. Kim, I. Alexeev, and H. M. Milchberg, Appl. Phys. Lett. **81**, 4124 (2002).
16. D. Patel, D. Jang, S. W. Hancock, H. M. Milchberg, and K.-Y. Kim, Opt. Express **28**, 11023 (2020).
17. S. Zahedpour, S. W. Hancock, and H. M. Milchberg, Opt. Lett. **44**, 843 (2019).
18. J. K. Wahlstrand, S. Zahedpour, A. Bahl, M. Kolesik, and H. M. Milchberg, Phys. Rev. Lett. **120**, 183901 (2018).
19. J. K. Wahlstrand, S. Zahedpour, and H. M. Milchberg, J. Opt. Soc. Am. B **33**, 1476 (2016).
20. J. K. Wahlstrand, Y.-H. Cheng, and H. M. Milchberg, Phys. Rev. A **85**, 043820 (2012).
21. Y.-H. Chen, S. Varma, A. York, and H. M. Milchberg, Opt. Express **15**, 11341 (2007).
22. M. Kolesik and J. V. Moloney, Phys. Rev. E **70**, 036604 (2004).
23. M. Kolesik, http://acms.arizona.edu/FemtoTheory/MK_personal/guppelab/.
24. X. M. Tong, Z. X. Zhao, and C. D. Lin, Phys. Rev. A **66**, 033402 (2002).
25. C. Guo, M. Li, J. P. Nibarger, and G. N. Gibson, Phys. Rev. A **58**, R4271 (1998).

REFERENCES

1. M. Kolesik, J. M. Brown, A. Teleki, P. Jakobsen, J. V. Moloney, and E. M. Wright, "Metastable electronic states and nonlinear response for high-intensity optical pulses," Optica **1**, 323–331 (2014).
2. A. Couairon and A. Mysyrowicz, "Femtosecond filamentation in transparent media," Phys. Rep. **441**, 47–189 (2007).
3. L. Bergé, S. Skupin, R. Nuter, J. Kasparian, and J.-P. Wolf, "Ultrashort filaments of light in weakly ionized optically transparent media," Rep. Prog. Phys. **70**, 1633–1713 (2007).
4. J. Kasparian and J.-P. Wolf, "Physics and applications of atmospheric nonlinear optics and filamentation," Opt. Express **16**, 466–493 (2008).
5. S. L. Chin, Femtosecond Laser Filamentation (Springer, 2009).
6. S. L. Chin, T.-J. Wang, C. Marceau, J. Wu, J. S. Liu, O. Kosareva, N. Panov, Y. P. Chen, J.-F. Daigle, S. Yuan, A. Azarm, W. W. Liu, T. Seideman, H. P. Zeng, M. Richardson, R. Li, and Z. Z. Xu, "Advances in intense femtosecond laser filamentation in air," Laser Phys. **22**, 1–53 (2012).
7. M. Kolesik and E. M. Wright, "Universal long-wavelength nonlinear optical response of noble gases," Opt. Express **27**, 25445–25456 (2019).
8. J. M. Brown, A. Lotti, A. Teleki, and M. Kolesik, "Exactly solvable model for non-linear light-matter interaction in an arbitrary time-dependent field," Phys. Rev. A **84**, 063424 (2011).
9. A. Bahl, J. M. Brown, E. M. Wright, and M. Kolesik, "Assessment of the metastable electronic state approach as a microscopically self-consistent description for the nonlinear response of atoms," Opt. Lett. **40**, 4987–4990 (2015).
10. A. Bahl, E. M. Wright, and M. Kolesik, "Nonlinear optical response of noble gases via the metastable electronic state approach," Phys. Rev. A **94**, 023850 (2016).
11. J. K. Wahlstrand, Y.-H. Cheng, and H. M. Milchberg, "High field optical nonlinearity and the Kramers-Kronig relations," Phys. Rev. Lett. **109**, 113904 (2012).
12. S. Zahedpour, J. K. Wahlstrand, and H. M. Milchberg, "Measurement of the nonlinear refractive index of air constituents at mid-infrared wavelengths," Opt. Lett. **40**, 5794–5797 (2015).
13. A. Bahl, J. K. Wahlstrand, S. Zahedpour, H. M. Milchberg, and M. Kolesik, "Nonlinear optical polarization response and plasma generation in noble gases: Comparison of metastable-electronic-state-approach models to experiments," Phys. Rev. A **96**, 043867 (2017).
14. J. M. Brown and M. Kolesik, "Properties of Stark resonant states in exactly solvable systems," Adv. Math. Phys. **2015**, 125832 (2015).
15. K. Y. Kim, I. Alexeev, and H. M. Milchberg, "Single-shot supercontinuum spectral interferometry," Appl. Phys. Lett. **81**, 4124 (2002).
16. D. Patel, D. Jang, S. W. Hancock, H. M. Milchberg, and K.-Y. Kim, "Simplified single-shot supercontinuum spectral interferometry," Opt. Express **28**, 11023–11032 (2020).
17. S. Zahedpour, S. W. Hancock, and H. M. Milchberg, "Ultrashort infrared 2.5-11μm pulses: spatiotemporal profiles and absolute nonlinear response of air constituents," Opt. Lett. **44**, 843–846 (2019).
18. J. K. Wahlstrand, S. Zahedpour, A. Bahl, M. Kolesik, and H. M. Milchberg, "Bound-electron nonlinearity beyond the ionization threshold," Phys. Rev. Lett. **120**, 183901 (2018).
19. J. K. Wahlstrand, S. Zahedpour, and H. M. Milchberg, "Optimizing the time resolution of supercontinuum spectral interferometry," J. Opt. Soc. Am. B **33**, 1476–1481 (2016).
20. J. K. Wahlstrand, Y.-H. Cheng, and H. M. Milchberg, "Absolute measurement of the transient optical nonlinearity in N_2, O_2, N_2O, and Ar," Phys. Rev. A **85**, 043820 (2012).
21. Y.-H. Chen, S. Varma, A. York, and H. M. Milchberg, "Single-shot, space- and time-resolved measurement of rotational wavepacket revivals in H_2, D_2, N_2, O_2, and N_2O," Opt. Express **15**, 11341–11357 (2007).
22. M. Kolesik and J. V. Moloney, "Nonlinear optical pulse propagation simulation: From Maxwell's to unidirectional equations," Phys. Rev. E **70**, 036604 (2004).
23. M. Kolesik, http://acms.arizona.edu/FemtoTheory/MK_personal/guppelab/.
24. X. M. Tong, Z. X. Zhao, and C. D. Lin, "Theory of molecular tunneling ionization," Phys. Rev. A **66**, 033402 (2002).
25. C. Guo, M. Li, J. P. Nibarger, and G. N. Gibson, "Single and double ionization of diatomic molecules in strong laser fields," Phys. Rev. A **58**, R4271–R4274 (1998).